

CRAP: Clutter Removal with Acquisitions Under Phase Noise

Marcus Henninger^{*†}, Silvio Mandelli^{*}, Artjom Grudnitsky^{*}, Thorsten Wild^{*}, Stephan ten Brink[†]

^{*}Nokia Bell Labs Stuttgart, 70469 Stuttgart, Germany

[†]Institute of Telecommunications, University of Stuttgart, 70569 Stuttgart, Germany

E-mail: marcus.henninger@nokia.com

Abstract—The emergence of Integrated Sensing and Communication (ISAC) in future 6G networks comes with a variety of challenges to be solved. One of those is clutter removal, which should be applied to remove the influence of unwanted components, scattered by the environment, in the acquired sensing signal. While legacy radar systems already implement different clutter removal algorithms, ISAC requires techniques that are tailored to the envisioned use cases and the specific challenges that communications deployments bring along, like phase noise due to clock errors between transmitter and receiver. To that end, in this work we introduce Clutter Removal with Acquisitions Under Phase Noise (CRAP). We propose to vectorize the time-frequency channel acquired in a radio frame in a high-dimensional space. In an offline clutter acquisition step, singular value decomposition is used to determine the major clutter components. At runtime, the clutter is then estimated and removed by a subspace projection of the acquired radio frame onto the clutter components.

Simulation results prove that CRAP offers benefits over prior art techniques robust to phase noise. In particular, our proposal does not suppress zero Doppler information, thereby enabling the detection of slow targets. Moreover, we show CRAP's real-time applicability in a millimeter-wave ISAC proof of concept, where a pedestrian is tracked in a cluttered lab environment.

I. INTRODUCTION

Integrated Sensing and Communication (ISAC) will be one of the main new features of future sixth generation (6G) systems [1] and is already part of discussions about later fifth generation (5G) releases. Current research is focusing, among others, on fundamental limits, use case definition, candidate waveforms, and spectrum usage [2], [3]. Whereas from an algorithmic perspective many approaches can be derived from conventional radar techniques, the peculiarities of communication systems together with the emerging use cases pose unique challenges and open up interesting research directions [4].

One such algorithmic task is clutter removal, which is applied to mitigate the effects of unwanted reflections due to objects in the environment that are not of interest for the sensing task. As this represents a long-known problem within the radar community, it has already been well researched in the past. Hence, various techniques exist, e. g., based on Moving Target Indication [5] or Space-Time Adaptive Processing [6],

to just name a few. Moreover, the Extensive Cancellation Algorithm (ECA) has been proposed [7], which works by projecting the signal into a subspace orthogonal to the clutter. In [8], Extensive Cancellation Algorithm by Subcarrier (ECA-C) has been introduced, which applies ECA to each carrier of a multi-carrier system, and can therefore in principle also be readily deployed in orthogonal frequency-division multiplexing (OFDM) radar systems.

However, most legacy radar operations differ significantly from the envisioned ISAC use cases [8]. For instance, conventional radars are usually only interested in (fast) moving objects, such as planes in airborne radar. Prior art clutter removal techniques therefore typically accept – or even intentionally create – suppression at zero Doppler [9], facilitating the detection of moving targets. Other approaches assume certain characteristics of the clutter, e. g., sea waves in [10], leveraging artificial intelligence to identify clutter. Those properties are clearly undesirable for many sensing applications currently being discussed in the context of ISAC, e. g., for tracking objects that are moving slowly or may even remain static for periods (humans, automated guided vehicles (AGVs)), with clutter of unknown characteristics.

In addition, classical communication setups have conceptual differences to conventional radars. For instance, the passive radars considered in [7] and [8] deploy a reference antenna steered towards the transmitter, while a surveillance antenna is steered into the direction to be surveyed by the system. In communication systems, such a reference is typically not available, rendering it difficult to adaptively estimate the clutter components. As a workaround, we rely on recording a reference scenario in an acquisition step, where only clutter components are present. To reduce the impact of noise and to capture multiple clutter components, several snapshots of the reference scenario are required. This, however, introduces phase incoherence, since in common communications hardware transmitter (TX) and receiver (RX) are not sharing the same local oscillator, posing another challenge that prior art clutter removal approaches have typically not been faced with.

This work addresses the aforementioned shortcomings with Clutter Removal with Acquisitions Under Phase Noise (CRAP). The main contribution are summarized as follows:

- We propose to perform clutter acquisition and removal by acquiring multiple OFDM symbols in a unique “radio frame”. This is compliant with the current 5G - and

This work has been submitted to the IEEE for possible publication. Copyright may be transferred without notice, after which this version may no longer be accessible.

likely 6G - frame structure. The radio frame is used to estimate the frame's channel state information (CSI) and vectorized, generating a multi-dimensional space. Multiple clutter acquisitions are then stacked in a matrix and used to determine the strongest clutter components using the singular value decomposition (SVD).

- The clutter is removed at runtime by subtracting, from the acquired radio frame, the projection of the acquired frame onto the clutter components.
- Exploiting the associative property of matrix multiplication, the computational complexity at runtime is drastically reduced, making the algorithm feasible for practical implementation.
- We demonstrate the benefits of CRAP both with simulation results, as well as with real-world measurements. Leveraging the proof of concept (PoC) shown in [11], pedestrian tracking results in a lab environment are shown, where CRAP has been applied in conjunction with a Kalman Filter (KF).

The rest of the paper is structured as follows: in Section II, we introduce the system model, before explaining CRAP in detail in Section III. Section IV demonstrates the benefits of CRAP by means of simulations. After presenting pedestrian tracking results obtained with our ISAC PoC in Section V, the paper is concluded in Section VI with a summary and a brief outlook at future work.

II. SYSTEM MODEL

To better introduce the problem at hand and to lay the necessary theoretical foundation, we first define a generic system model that can later also be linked to the ISAC PoC in Section V.

Consider a setup with separate TX and RX, where the TX transmits M OFDM symbols at carrier frequency f_c , with N subcarriers spaced by Δf carrying complex modulation symbols. Accordingly, the transmitted OFDM frame is represented by the matrix $\mathbf{X} \in \mathbb{C}^{N \times M}$. For simplicity, we consider co-located TX and RX in the following. Note, however, that our approach does not rely on a specific model, but can also be applied to bi-static or even distributed scenarios. Each object in the environment indexed $p \in \mathcal{P}$ is characterized by its range r_p and velocity v_p relative to the RX. These objects are partitioned into the sets $\mathcal{P}_c \subset \mathcal{P}$ and $\mathcal{P}_t \subset \mathcal{P}$, comprising clutter components and targets, respectively. The received frame $\mathbf{Y} \in \mathbb{C}^{N \times M}$ at the RX can then be seen as the superposition of all reflections of the signal with the objects in the environment. Assuming knowledge of the transmitted symbols \mathbf{X} at the RX, the time-frequency CSI matrix is obtained via element-wise division of \mathbf{Y} by \mathbf{X} and given as

$$\mathbf{H} = \phi \sum_{p \in \mathcal{P}} \alpha_p \mathbf{a}(r_p) \mathbf{b}(v_p)^T + \mathbf{Z}, \quad (1)$$

with α_p being the complex coefficient of the p -th reflection. Further, $\mathbf{Z} \in \mathbb{C}^{N \times M}$ denotes the random complex additive white Gaussian noise (AWGN) matrix, where we define each element to have a power of $\sigma_n^2 = P_n/N$, with P_n representing

the noise power over the full bandwidth. The vectors $\mathbf{a}(r_p)$ and $\mathbf{b}(v_p)$ are written as

$$\mathbf{a}(r_p) = [1, e^{-j4\pi\Delta f \cdot r_p/c}, \dots, e^{-j4\pi(N-1)\Delta f \cdot r_p/c}]^T \quad (2)$$

$$\mathbf{b}(v_p) = [1, e^{j4\pi T_0 f_c \cdot v_p/c}, \dots, e^{j4\pi(M-1)T_0 f_c \cdot v_p/c}]^T \quad (3)$$

where c is the speed of light and T_0 the OFDM symbol duration. Moreover, ϕ denotes the random phase rotation, which is modeled to be constant within a single sensing acquisition \mathbf{H} . This can be safely assumed if the phase noise random walk's standard deviation during an acquisition of one frame is $\sigma_\phi < 0.1$ rad [12], which is typically the case in the ISAC demonstrator based on communications hardware we introduced in [11]. Note that the phase rotation between consecutive frames does not need to be constrained to any value, nor model, in order for our approach to be valid.

Information about the objects' velocities v_p and ranges r_p is contained in \mathbf{H} in the form of linear phase shifts in time and frequency domain, respectively. The CSI matrix can thus in principle be readily processed using conventional OFDM radar techniques [13] to extract knowledge about reflective objects in the environment. However, as previously mentioned, reflections from the unwanted components in the set \mathcal{P}_c , such as reflections caused by (typically static) objects which are not of interest for the sensing task, are also included in the sensing acquisition. Their influence should be removed, calling for the application of clutter removal algorithms.

III. CRAP

This section describes our proposed solution to the previously outlined clutter removal problem in detail. Our algorithm, CRAP, can be seen as a two-step approach.

First, in an "offline" acquisition step, the matrices required for clutter removal are generated by recording multiple snapshots of the reference scenario (i. e., where only clutter is present) and then extracting the meaningful clutter components. During runtime, those matrices are utilized to compute the clutter-rejected channel building upon the principles of ECA [7].

A. Clutter Acquisition (Offline)

To capture multiple clutter components and to reduce the impact of noise, K snapshots of the reference scenario are initially recorded. After vectorizing those K CSI matrices, the resulting vectors of length $Q = NM$ are stacked along the rows to form the matrix $\mathbf{C} \in \mathbb{C}^{K \times Q}$ comprising all vectorized clutter acquisitions. Notice that doing so merely collapses the representation of the clutter into a vector, but preserves all the information, such that later clutter projection and removal can exploit the multi-dimensional space of the CSI. In contrast, ECA-C [8] operates across a *single* domain, the time domain, thereby suppressing zero Doppler information when removing the clutter, as shown in Section V.

To relax the computational complexity at runtime, only meaningful clutter components should be considered. To that end, the SVD of the clutter matrix \mathbf{C} is performed as

$$\mathbf{C} = \mathbf{U}\mathbf{\Sigma}\mathbf{V}^H. \quad (4)$$

Algorithm 1: Clutter Acquisition (Offline)

Input: K clutter acquisition frames,
optional: clutter order L

Output: Clutter removal matrices \mathbf{P}' , $\hat{\mathbf{C}}^H$

- 1: $\mathbf{C} \leftarrow$ vectorize and stack K clutter acquisitions
 - 2: Σ , $\mathbf{V}^H \leftarrow$ perform SVD with Eq. (4)
 - 3: **if** L not specified **then**
 - 4: $L \leftarrow$ estimate clutter order using singular values Σ
 - 5: **end if**
 - 6: $\hat{\mathbf{C}} \leftarrow$ store L strongest right singular vectors from \mathbf{V}^H
 - 7: $\mathbf{P}' \leftarrow$ compute part of projection matrix using Eq. (6)
 - 8: **return** \mathbf{P}' , $\hat{\mathbf{C}}^H$
-

The clutter order L can either be chosen beforehand, or determined by means of the singular values in Σ , e. g., using Minimum Description Length (MDL) [14]. The right singular vectors (i. e., rows) of \mathbf{V}^H corresponding to the L strongest singular values are then stacked along the columns to obtain the matrix $\hat{\mathbf{C}} \in \mathbb{C}^{Q \times L}$, which we consider to be the clutter subspace containing the L strongest clutter components. It is hereby crucial to remark that phase fluctuations between different clutter acquisitions do not affect the singular vectors, which allows obtaining robust representations of the clutter subspace even in case of clock incoherence between TX and RX.

The clutter subspace $\hat{\mathbf{C}}$ alone in principle already allows to obtain the clutter projection at runtime as

$$\hat{\mathbf{c}} = \overbrace{\hat{\mathbf{C}}(\hat{\mathbf{C}}^H\hat{\mathbf{C}})^{-1}\hat{\mathbf{C}}^H}^{\mathbf{P}} \mathbf{h} \quad (5)$$

where the matrix \mathbf{P} projecting the vectorized sensing acquisition \mathbf{h} into the clutter subspace can be computed fully offline. However, determining \mathbf{P} results in a $Q \times Q$ matrix, which is typically too large to perform clutter removal in real time. We therefore leverage the associative property of matrix multiplication to avoid the explicit computation of \mathbf{P} by performing the multiplications in the following order

$$\hat{\mathbf{c}} = \overbrace{[\hat{\mathbf{C}}(\hat{\mathbf{C}}^H\hat{\mathbf{C}})^{-1}]^{\mathbf{P}'}} (\hat{\mathbf{C}}^H\mathbf{h}) . \quad (6)$$

Clutter projection performed as per Eq. (6) requires the Hermitian transpose of the clutter subspace $\hat{\mathbf{C}}^H \in \mathbb{C}^{L \times Q}$ and part of the projection matrix $\mathbf{P}' \in \mathbb{C}^{Q \times L}$. Those matrices can be pre-computed and stored, relaxing the computational burden, as typically $L \ll Q$. This further emphasizes the necessity of isolating the strongest clutter components and keeping L small. The entire procedure of CRAP's clutter acquisition step is given in Algorithm 1.

B. Clutter Removal (Runtime)

During runtime, the clutter-rejected sensing acquisition $\hat{\mathbf{h}}$ is obtained by subtracting the clutter projection from the current vectorized CSI

$$\hat{\mathbf{h}} = \mathbf{h} - \mathbf{P}'(\hat{\mathbf{C}}^H\mathbf{h}) . \quad (7)$$

Algorithm 2: Clutter Removal (Runtime)

Input: Clutter removal matrices \mathbf{P}' , $\hat{\mathbf{C}}^H$,
current sensing acquisition \mathbf{H}

Output: Clutter-rejected sensing acquisition $\hat{\mathbf{H}}$

- 1: $\mathbf{h} \leftarrow$ vectorize current sensing acquisition \mathbf{H}
 - 2: $\hat{\mathbf{h}} \leftarrow$ get clutter-rejected sensing acquisition using \mathbf{P}' , $\hat{\mathbf{C}}^H$, and Eq. (7)
 - 3: $\hat{\mathbf{H}} \leftarrow$ reshape clutter-rejected sensing acquisition
 - 4: **return** $\hat{\mathbf{H}}$
-

Reshaping $\hat{\mathbf{h}}$ into its original shape finally yields the clutter-rejected CSI matrix $\hat{\mathbf{H}}$, which is further used for OFDM radar processing. Algorithm 2 summarizes the clutter removal step at runtime.

Notice that our algorithm can straightforwardly be extended to further dimensions, e. g., by considering also the angular domain (multiple antennas).

C. A note on computational complexity

CRAP's computational bottleneck is clearly the SVD of the $K \times Q$ matrix \mathbf{C} in (4). This can however be tolerated, as the first step of our approach is performed completely "offline". The runtime complexity of our proposed solution then scales linearly with QL , hence with Q , as typically $L \ll Q$, which has proven to be sufficient for real-time implementation. However, one could still apply decimation techniques to undersample the CSI matrix and get $Q' \ll Q$ to further reduce complexity. In that case, interpolation techniques may be applied to $\hat{\mathbf{H}}$ after clutter removal to "recover" the information lost by under-sampling, e. g., based on the principles of [15]. This could be of particular interest in case the application of the algorithm is extended to further dimensions.

IV. SIMULATION RESULTS

This section will demonstrate the benefits of CRAP by means of simulation results. We first describe our simulation setup and the considered baselines, which are then compared to CRAP in terms of target detection and root-mean-square error (RMSE) performance.

A. Simulation Setup

For our simulation campaign, we consider the system model described in Section II with co-located TX and RX, each with a single antenna.

We randomly place $|\mathcal{P}_c| = 5$ static clutter components in the environment, which is in line with the number of multipath clusters that can be expected in an indoor environment [16]. Note that we assume $|\mathcal{P}_c|$ to be known such that L is chosen to be 5. As previously mentioned and also later done in our PoC experiments in Section V, L may in practice be estimated based on the singular values using model order estimation algorithms such as MDL. During the clutter acquisition phase, the clutter contributions are captured with $K = 100$ snapshots.

TABLE I. SIMULATION PARAMETERS.

Number of subcarriers N	1584
Number of OFDM symbols per radio frame M	1120
Carrier frequency f_c	27.4 GHz
Subcarrier spacing Δf	120 kHz
Total bandwidth B	190 MHz
Number of clutter components $ \mathcal{P}_c $	5
Number of clutter acquisitions K	100
Probability of false alarm P_{FA}	0.001

For each experiment, a single target, whose presence is to be detected by the sensing system, is added to the scenario at a random range at runtime. The target's velocities are uniformly drawn between -1.5 m/s and 1.5 m/s, corresponding to a typical pedestrian tracking use case. Note that we confine the maximum one-way distance between all objects and the radar to 25 m. The complex coefficients α_p of all objects are generated according to a Rician distribution, and free-space path loss is considered to model their attenuation. In our simulations, we also consider noise powers below the thermal noise floor $P_n^* = -174 \frac{\text{dBm}}{\text{Hz}} \cdot B \approx 91 \text{ dBm}$ to investigate the performance at higher signal-to-noise ratios (SNRs), which can occur in other scenarios, e. g., in case of higher transmit powers, closer targets, or larger radar cross-sections.

The Radio frequency (RF) parameters chosen for the simulation study are closely coupled to our millimeter-wave (mmWave) ISAC PoC. Each of the K acquisitions comprises $M = 1120$ symbols, corresponding to the number of symbols per radio frame for the numerology that was also used in our demonstrator [17]. A summary of the simulation parameters can be found in Table I.

We compare CRAP to the following baselines:

1) **“ECA-C”**: As mentioned earlier, ECA-C [8] is the closest prior art and works by projecting and removing the clutter per subcarrier. This modified version of ECA-C uses the same K clutter acquisitions, but does not apply vectorization and instead performs clutter removal per subcarrier. The clutter-rejected n -th carrier is given as

$$\hat{\mathbf{h}}_{c,n}^T = \mathbf{H}(n, :) - \mathbf{H}(n, :) \mathbf{C}_{c,n}^H (\mathbf{C}_{c,n} \mathbf{C}_{c,n}^H)^{-1} \mathbf{C}_{c,n} \quad (8)$$

with $\mathbf{H}(n, :)$ being the n -th row, i. e., subcarrier, of the current sensing acquisition. Further, $\mathbf{C}_{c,n} \in \mathbb{C}^{K \times M}$ denotes the n -th clutter matrix, which is obtained by stacking the n -th carrier's K clutter acquisition vectors of length M along the rows. The full clutter-rejected sensing acquisition after applying ECA-C is then $\hat{\mathbf{H}}_{\text{ECA-C}} = [\hat{\mathbf{h}}_{c,1} \ \hat{\mathbf{h}}_{c,2} \ \dots \ \hat{\mathbf{h}}_{c,N}]^T$.

2) **“ECA-S”**: As another baseline, we propose Extensive Cancellation Algorithm by Symbol (ECA-S). This technique relies on the same principles as ECA-C, but leverages the multicarrier nature of the OFDM signal and performs clutter removal on each *symbol*, i. e., it simply operates in the frequency domain instead of the time domain as ECA-C. Hence, the clutter-rejected m -th symbol is

$$\hat{\mathbf{h}}_{s,m} = \mathbf{H}(:, m) - \mathbf{C}_{s,m} (\mathbf{C}_{s,m}^H \mathbf{C}_{s,m})^{-1} \mathbf{C}_{s,m}^H \mathbf{H}(:, m) \quad (9)$$

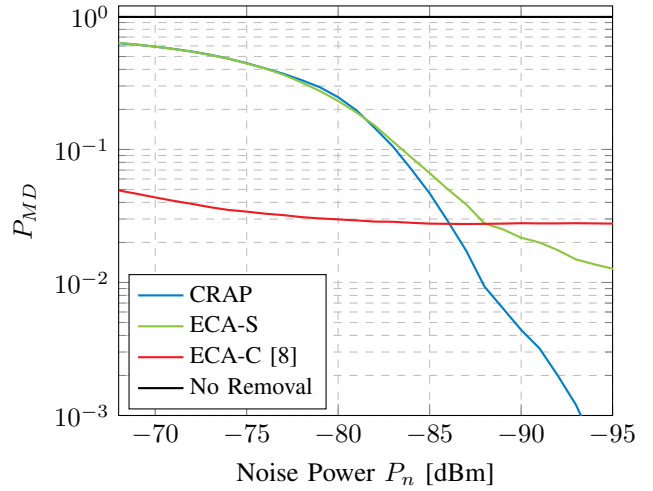


Fig. 1: Probability of missed detection for our proposal “CRAP”, baselines “ECA-C” and “ECA-S”, as well as “No Removal”, i. e., without any clutter removal applied.

where $\mathbf{H}(:, m)$ extracts the m -th column (symbol) out of \mathbf{H} . The clutter matrix $\mathbf{C}_{s,m} \in \mathbb{C}^{N \times K}$ is now constructed by stacking the m -th symbol's K clutter acquisition vectors of length N along the columns. The complete clutter-rejected sensing acquisition with ECA-S is written as $\hat{\mathbf{H}}_{\text{ECA-S}} = [\hat{\mathbf{h}}_{s,1} \ \hat{\mathbf{h}}_{s,2} \ \dots \ \hat{\mathbf{h}}_{s,M}]$.

3) **“No Removal”**: Finally, we consider also the case without applying any clutter removal algorithm, i. e., target detection is performed directly on the unprocessed sensing acquisition \mathbf{H} .

The respective clutter-rejected CSI matrices are then further processed using OFDM radar principles to estimate the target's range and velocity. A maximum likelihood estimate of the parameters can be found by evaluating the periodogram, which is obtained by performing a Discrete Fourier Transform (DFT) over the OFDM symbols and an Inverse Discrete Fourier Transform (IDFT) over the subcarriers of $\hat{\mathbf{H}}$ [13]

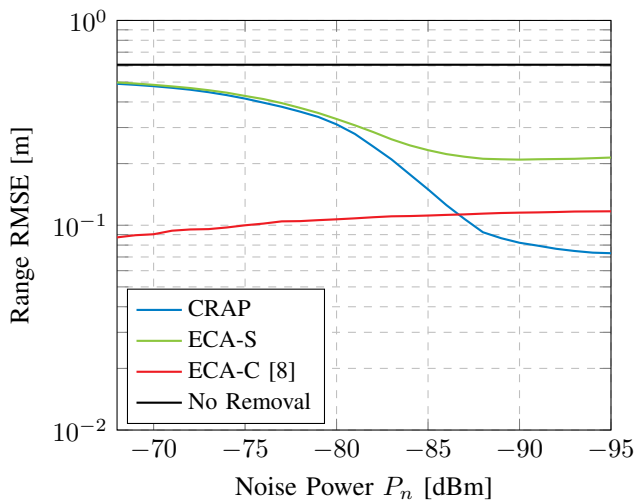
$$S(n, m) = \frac{1}{N'M'} \left| \sum_{k=0}^{N'} \left(\sum_{l=0}^{M'} \hat{\mathbf{H}}(k, l) e^{-j2\pi \frac{lm}{M'}} \right) e^{j2\pi \frac{kn}{N'}} \right|^2 \quad (10)$$

where $N' = 2^{\lceil \log_2 N \rceil}$ and $M' = 2^{\lceil \log_2 M \rceil}$ denote the number of rows and columns of $\hat{\mathbf{H}}$ after zero padding.

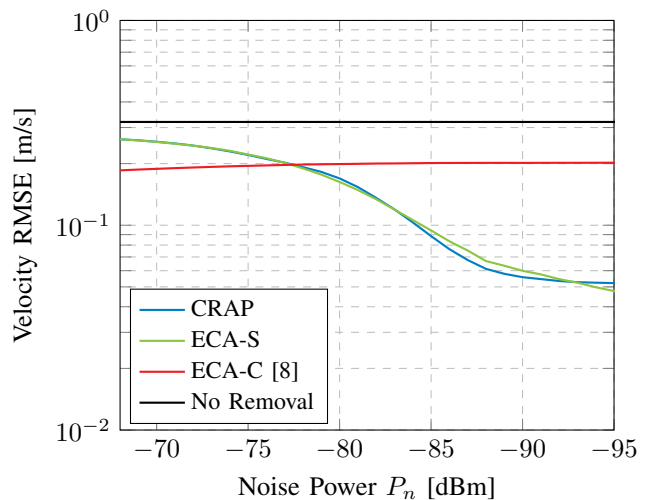
As multi-peak detection and matching techniques are not the scope of this work, we restrict to the detection of only the strongest peak. Accordingly, the indices of the strongest periodogram bin are found as

$$(\hat{n}, \hat{m}) = \arg \max_{n, m} S(n, m) . \quad (11)$$

We consider the peak to be a detection if $S(\hat{n}, \hat{m})$ exceeds a constant false alarm rate (CFAR) threshold η defined by a pre-determined probability of false alarm P_{FA} . The target's range \hat{r} and speed \hat{v} estimates are obtained by applying interpolation to the bin indices, and converting the resulting fractional indices to range and Doppler values as described in [18].



(a) Range RMSE.



(b) Velocity RMSE.

Fig. 2: Range and velocity RMSE for our proposal “CRAP, baselines “ECA-C” and “ECA-S”, as well as “No Removal”, i. e., without any clutter removal applied.

B. Detection Performance

We now evaluate CRAP’s target detection capabilities compared to the previously defined baselines “ECA-C”, “ECA-S”, and “No Removal”. All approaches are evaluated in terms of the probability of missed detection P_{MD} , defined as the percentage of undetected targets. Note that we only consider a peak a detection if both its range and speed errors are smaller than their corresponding theoretical resolutions, which are given as $\Delta r = \frac{c}{2N\Delta f}$ and $\Delta v = \frac{c\Delta f}{2Mf_c}$, respectively [18].

Fig. 1 displays the missed detection probability curves. First, it can be noticed that without clutter removal (“No Removal”) the missed detection probability is close to one, as typically a clutter component causes the strongest reflection. One can further observe that, while “ECA-C” offers the best detection capabilities for high noise powers, its P_{MD} saturates quickly. This can be attributed to the zero Doppler suppression effect, leaving (almost) static targets undetected. We will further illustrate this behavior by means of a real-world example in Section V. A similar saturation effect can also be noticed for “ECA-S”. These missed detections are due to “ECA-S” operating only in the frequency domain, and occur when the target is at the same range as a strong clutter component. This can be seen as the analogue to the attenuation at zero Doppler that is created by ECA-C due to static clutter.

Our proposal “CRAP”, on the other side, does not exhibit such a saturation effect. Once the noise power is low enough that the K acquisitions allow to completely capture the clutter components, their influence can be removed without canceling the true target. Whereas the exact extents of the ECA-C/ECA-S saturation effects clearly depend on the clutter components, thus on the scenario, it can be stated that CRAP is the only technique that does not impose requirements on target or clutter characteristics. Moreover, it is worth noting that the SNR in the low noise power regimes, i. e., where “CRAP”

performs best, can typically be assumed in sensing applications thanks to the available processing gain (due to the 2D DFT) or beamforming gains, as in real demonstrators [11].

C. RMSE Performance

Next, the RMSE performance is investigated. To that end, the RMSE for parameter Θ (either range r or velocity v) is defined as

$$\text{RMSE} = \sqrt{E_j [|\hat{\Theta}_j - \Theta_j|^2]} \quad (12)$$

where $\hat{\Theta}_j$ and Θ_j are estimate and true value of the respective parameter in the j -th experiment. Note that in case of a missed detection, we assume an error equal to the respective DFT bin width (in terms of range and velocity).

Fig. 2 displays the range and velocity RMSE curves of the investigated techniques. “CRAP” converges to range and speed errors of ca. 0.07 m and 0.05 m/s, respectively, once no missed detections occur anymore. “ECA-S” offers similar velocity estimation capabilities as “CRAP”, but suffers in the range estimation. The adverse effect is observed for “ECA-C”, which offers an almost equal range estimation performance as “CRAP”, but loses in velocity estimation. Again, this can be attributed to the fact that ECA-C and ECA-S perform clutter removal only in time and frequency domain, respectively, thereby causing performance degradation in the respective dimension.

V. POC RESULTS

To evaluate CRAP, we integrate it as part of our ISAC PoC, and use the system to track the movement of a pedestrian.

The PoC is built on top of a 5G gNodeB (gNB) operating in FR2 (27.4 GHz carrier frequency) with a 200 MHz carrier and $\mu = 3$ numerology, consistent with the parameters in Table I.

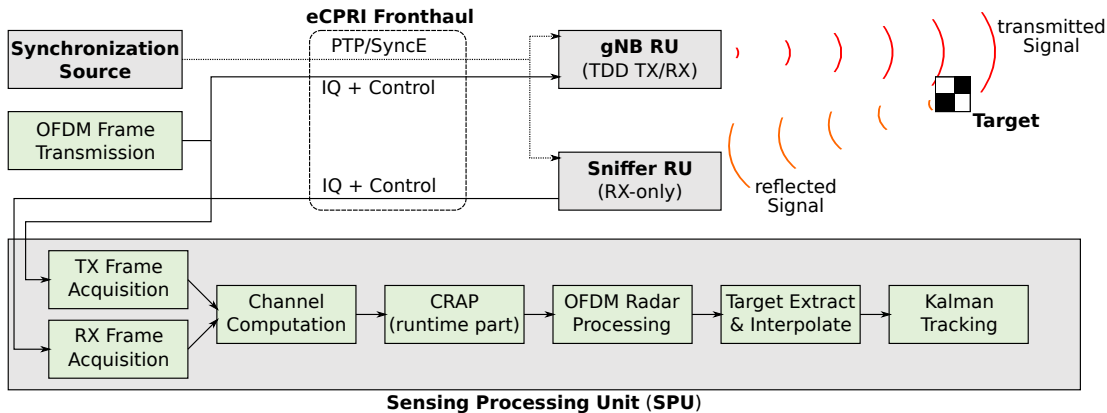


Fig. 3: ISAC PoC schematic with main processing blocks and interfaces.

We use a 64-QAM modulated downlink signal, transmitted using a 4:1 downlink (DL)/uplink (UL) frame structure [17].

As our radio hardware is not full-duplex capable, we are using quasi co-located TX and RX as in Fig. 4, properly isolated to avoid self-interference. Both transceivers are analog uniform rectangular arrays with 16×16 antenna elements, separated by half a wavelength. Both Radio Units (RUs) are synchronized using a combination of Precision Timing Protocol (PTP) [19] and Synchronous Ethernet (SyncE) [20], with a measured synchronization jitter of approx. 33 ps (standard deviation). Still, even this level of synchronization precision means that there is noticeable phase incoherence (ϕ) between the transmitted and reflected signals, as described in the system model in Section II, and addressed in Section III-A. In our setup, however, the phase noise standard deviation during a radio frame acquisition σ_ϕ is such that periodogram operations can be performed with negligible distortion.

We acquire the transmitted signals by monitoring the fronthaul to the gNB RU and stream that along with the reflected signal from the Sniffer RU into a real-time OFDM radar, which performs the following steps:

- TX/RX Radio Frame Acquisition, result: Matrices of TX/RX Signals for full radio frame
- Channel Computation, result: Channel matrix
- CRAP (runtime part), result: Clutter-rejected channel matrix
- OFDM Radar Processing, result: 2D-Periodogram
- Target Extraction and Interpolation, result: Target list
- Kalman Tracking, result: Modified range and speed for one target

Additionally, the implementation allows recording transmitted and reflected signals to allow (i) offline OFDM Radar Processing and (ii) Clutter Acquisition as described in Section III-A. An overview of the ISAC PoC with its main processing blocks is given in Fig. 3. A more detailed description of the PoC realization, can be found in [11].

For tracking the pedestrian, we deploy a simple KF [21], which tracks the status $\mathbf{x}_i = [r_i, v_i]$ at time i , where r_i and v_i are the KF posterior range and speed estimates at time i ,

respectively. The KF is initialized as $\mathbf{x}_0 = [\hat{r}_0, \hat{v}_0]^T$ after the first detection. Then, using a constant velocity motion model, the predicted state vector and covariance at time index i are computed as

$$\hat{\mathbf{x}}_{i|i-1} = \begin{bmatrix} 1 & \Delta t \\ 0 & 1 \end{bmatrix} \mathbf{x}_{i-1|i-1} \quad (13)$$

$$\hat{\mathbf{P}}_{i|i-1} = \begin{bmatrix} 1 & \Delta t \\ 0 & 1 \end{bmatrix} \mathbf{P}_{i-1|i-1} \begin{bmatrix} 1 & 0 \\ \Delta t & 1 \end{bmatrix} + \mathbf{Q} \quad (14)$$

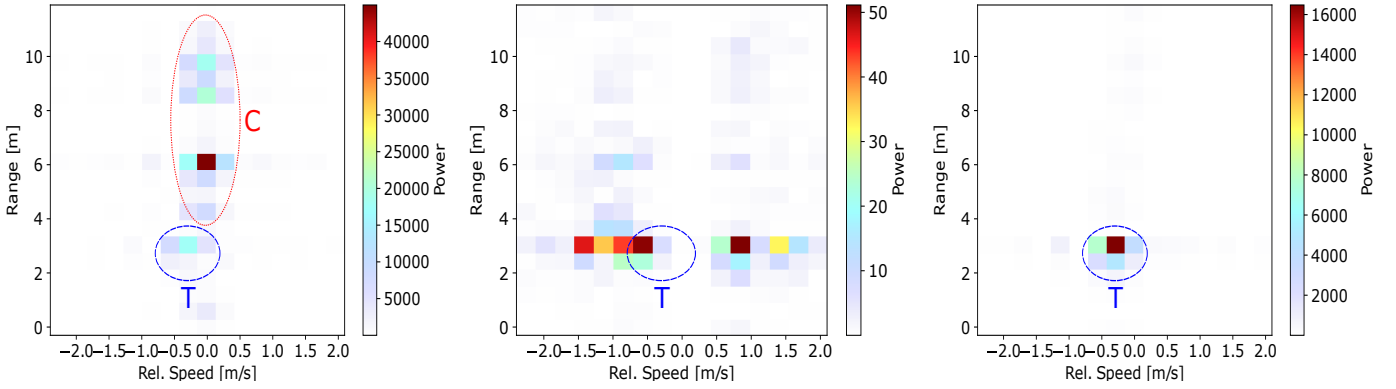
where \mathbf{Q} is the process noise covariance and Δt the time between measurements, which in our experiments corresponds to 10 ms (duration of one radio frame). Assuming a linear measurement model where the state is directly observed with AWGN, the current observation $\mathbf{z}_i = [\hat{r}_i, \hat{v}_i]^T$ is fed to the KF in the update step to obtain the a posteriori state vector and covariance matrix as

$$\mathbf{x}_{i|i} = \hat{\mathbf{x}}_{i|i-1} + \mathbf{K}_i (\mathbf{z}_i - \hat{\mathbf{x}}_{i|i-1}) \quad (15)$$

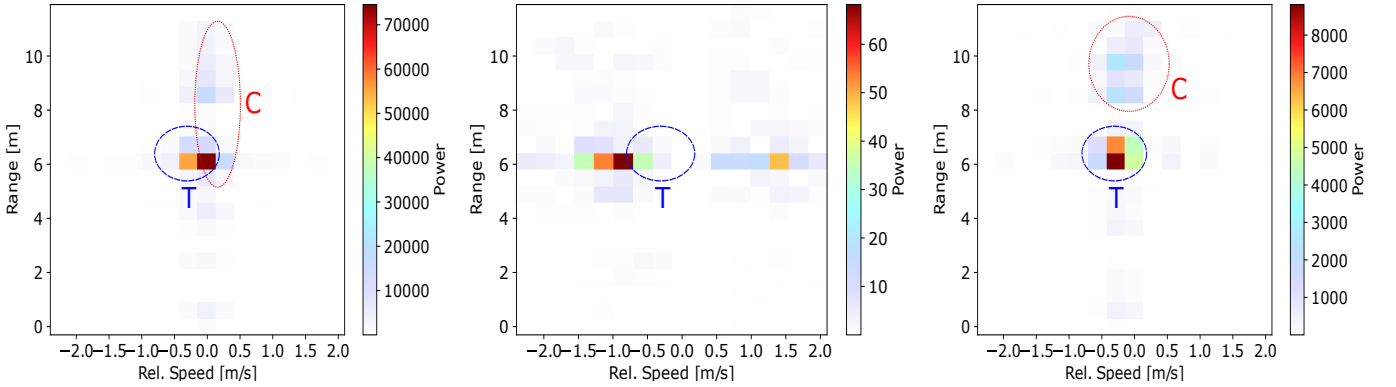
$$\mathbf{P}_{i|i} = (\mathbf{I} - \mathbf{K}_i) \hat{\mathbf{P}}_{i|i-1} \quad (16)$$



Fig. 4: Human target **T** walking away from the ISAC PoC in the direction of the strong clutter component **C**.



(a) no clutter removal, pedestrian at range of ca. 3 m. (b) clutter removal with ECA-C, pedestrian at range of ca. 3 m. (c) clutter removal with CRAP, pedestrian at range of ca. 3 m.



(d) no clutter removal, pedestrian close to clutter at range of ca. 6 m. (e) clutter removal with ECA-C, pedestrian close to clutter at range of ca. 6 m. (f) clutter removal with CRAP, pedestrian close to clutter at range of ca. 6 m.

Fig. 5: Periodograms of sensing acquisition without applying clutter removal (left), clutter removal with “ECA-C” (middle), and clutter removal using our proposal “CRAP” (right). In the first row, the human target **T** is walking at a range of ca. 3 m, in the second row close to the strong clutter component **C** at a range of ca. 6 m.. Both “ECA-C” and “CRAP” remove the clutter well, but only “CRAP” does not create suppression at zero Doppler, enabling the detection of the slow moving target.

where $\mathbf{K}_i = \hat{\mathbf{P}}_{i|i-1}(\hat{\mathbf{P}}_{i|i-1} + \mathbf{R}_i)^{-1}$ is the Kalman gain with \mathbf{R}_i denoting the measurement noise covariance [21].

The KF is reset 1) in case of a timeout (time since last detection $> T_{\max} = 0.5$ s), or 2) if either its range or speed standard deviation exceeds the pre-defined upper bound of $\sigma_{r,\max} = 2$ m and $\sigma_{v,\max} = 2$ m/s, respectively.

The results discussed in the following are obtained from experiments in our lab, where a pedestrian was walking from the sensing system in the direction of the strong clutter component as shown in Fig. 4. This is the underlying scenario for all PoC results discussed hereinafter.

A. Clutter Removal Example

We first demonstrate the benefits of CRAP by means of range-speed periodogram visualizations of a single sensing acquisition from our ISAC PoC pedestrian tracking experiments. As in Sec. IV, $K = 100$ clutter acquisitions were recorded. Here, however, we estimated the clutter order using MDL for which $L = 3$ was obtained.

Fig. 5 visualizes the periodograms of a single radio frame for two different scenarios: in the figures of the first row, the

human target **T** is moving at a range of ca. 3 m from the RU, whereas the second row shows periodograms with the pedestrian walking close to the strong clutter **C** (metal cabinet), comparable to Fig. 4. One can discern that without clutter removal (Figs. 5a and 5d) the most energy is backscattered by the metal cabinet in both scenarios, which further underlines the necessity of proper clutter removal techniques in practice. The periodograms after applying clutter removal with “ECA-C” are displayed in the middle (Figs. 5b and 5e). Due to the strong static clutter, a deep null at zero Doppler is created, impacting also the slow moving pedestrian and thereby impeding its detection. While some residual target contributions remain, their energy is much lower (note the different color scales for each periodogram), rendering the detection of the pedestrian difficult. Moreover, the remaining peaks are shifted due to the attenuation at zero Doppler, which leads to an increased velocity estimation error (cf. also Fig. 2b).

The figures in the right column (Figs. 5c and 5f) depict the periodograms after applying clutter removal according to our proposal “CRAP”. The reflection caused by the pedestrian is

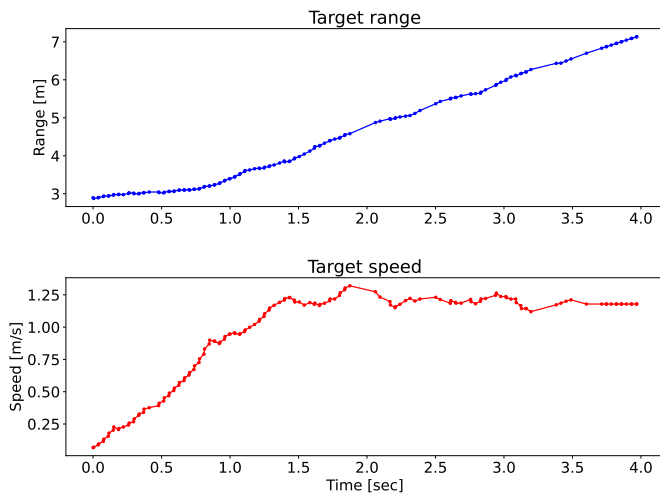


Fig. 6: Range (above) and speed (below) of a pedestrian tracked by the ISAC PoC in a real-world lab environment. CRAP is used for clutter removal and a KF is used for post-processing the strongest peak extracted from the periodogram.

now the strongest contribution that remains in the periodogram in both figures. Fig. 5f demonstrates that CRAP is still able to isolate a target even if it is walking slowly and very close to the strong clutter component, although compared to Fig. 5c more residual clutter contributions remain. This allows the detection of the pedestrian with the peak search described in Section IV without the need for processing other peaks caused by clutter.

B. Pedestrian Tracking Example

Finally, Fig. 6 shows an excerpt with a duration of 4 s of a pedestrian’s range and speed being tracked in our lab with the ISAC PoC. One can observe that our system is able to track the pedestrian’s movement stably without being impacted by the reflections caused by the strong clutter (metal cabinet in Fig. 4) or other backscattering components thanks to the use of CRAP.

VI. CONCLUSION

In this work, we proposed a clutter removal algorithm named CRAP, which is robust to phase noise and preserves zero Doppler information. Our simulation study showed that the missed detection probability can be reduced by at least one order of magnitude in high SNR regimes, which will likely be available in real scenarios. Moreover, we demonstrated pedestrian tracking results obtained with our ISAC PoC that deploys CRAP in conjunction with a KF, which further emphasize CRAP’s benefits and real-time capability. Future work should investigate decimation and interpolation techniques to further reduce the computational complexity during clutter acquisition, as well as the extension of CRAP to also include the angular domain.

ACKNOWLEDGMENTS

We would like to thank Frank Schaich and Junqing Guan for their insights and feedback during this work’s development and implementation in the ISAC PoC.

This work was developed within the KOMSENS-6G project, partly funded by the German Ministry of Education and Research under grant 16KISK112K.

REFERENCES

- [1] T. Wild, V. Braun, and H. Viswanathan, “Joint design of communication and sensing for beyond 5G and 6G systems,” *IEEE Access*, vol. 9, pp. 30 845–30 857, 2021.
- [2] S. Mandelli, M. Henninger, M. Bauhofer, and T. Wild, “Survey on Integrated Sensing and Communication Performance Modeling and Use Cases Feasibility,” *arXiv 2305.07144*, 2023. [Online]. Available: <https://arxiv.org/abs/2305.07144>
- [3] J. A. Zhang, M. L. Rahman, K. Wu, X. Huang, Y. J. Guo, S. Chen, and J. Yuan, “Enabling joint communication and radar sensing in mobile networks—A survey,” *IEEE Communications Surveys & Tutorials*, vol. 24, no. 1, pp. 306–345, 2021.
- [4] D. K. P. Tan, J. He, Y. Li, A. Bayesteh, Y. Chen, P. Zhu, and W. Tong, “Integrated sensing and communication in 6G: Motivations, use cases, requirements, challenges and future directions,” in *2021 1st IEEE International Online Symposium on Joint Communications & Sensing (JC&S)*. IEEE, 2021, pp. 1–6.
- [5] M. Ash, M. Ritchie, and K. Chetty, “On the application of digital moving target indication techniques to short-range FMCW radar data,” *IEEE Sensors Journal*, vol. 18, no. 10, pp. 4167–4175, 2018.
- [6] S. Sen, “OFDM Radar Space-Time Adaptive Processing by Exploiting Spatio-Temporal Sparsity,” *IEEE Transactions on Signal Processing*, vol. 61, no. 1, pp. 118–130, 2012.
- [7] F. Colone, D. O’Hagan, P. Lombardo, and C. Baker, “A multistage processing algorithm for disturbance removal and target detection in passive bistatic radar,” *IEEE Transactions on aerospace and electronic systems*, vol. 45, no. 2, pp. 698–722, 2009.
- [8] Z. Zhao, X. Wan, Q. Shao, Z. Gong, and F. Cheng, “Multipath clutter rejection for digital radio mondiale-based HF passive bistatic radar with OFDM waveform,” *IET Radar, Sonar & Navigation*, vol. 6, no. 9, pp. 867–872, 2012.
- [9] Y. Liu, J. Yi, X. Wan, X. Zhang, and H. Ke, “Evaluation of clutter suppression in CP-OFDM-based passive radar,” *IEEE Sensors Journal*, vol. 19, no. 14, pp. 5572–5586, 2019.
- [10] T. Islam, M. A. Rico-Ramirez, D. Han, and P. K. Srivastava, “Artificial intelligence techniques for clutter identification with polarimetric radar signatures,” *Atmospheric Research*, vol. 109, pp. 95–113, 2012.
- [11] T. Wild, A. Grudnitsky, S. Mandelli, M. Henninger, J. Guan, and F. Schaich, “6G Integrated Sensing and Communication: From Vision to Realization,” *arXiv 2305.01978*, 2023. [Online]. Available: <https://arxiv.org/abs/2305.01978>
- [12] S. Mandelli, M. Magarini, and A. Spalvieri, “Modeling the Filtered and Sampled Continuous-time Signal Affected by Wiener Phase Noise,” in *2014 19th European Conference on Networks and Optical Communications-(NOC)*. IEEE, 2014, pp. 173–178.
- [13] M. Braun, C. Sturm, and F. K. Jondral, “Maximum likelihood speed and distance estimation for OFDM radar,” in *2010 IEEE Radar Conference*. IEEE, 2010, pp. 256–261.
- [14] J. Rissanen, “Modeling by shortest data description,” *Automatica*, vol. 14, no. 5, 1978.
- [15] S. Mandelli, M. Henninger, and J. Du, “Sampling and Reconstructing Angular Domains with Uniform Arrays,” *IEEE Transactions on Wireless Communications*, early access. doi: 10.1109/TWC.2022.3220045.
- [16] N. Czink, M. Herdin, H. Özcelik, and E. Bonek, “Number of multipath clusters in indoor MIMO propagation environments,” *Electronics letters*, vol. 40, no. 23, pp. 1498–1499, 2004.
- [17] 3GPP, “NR; Physical channels and modulation,” Technical Specification (TS) 38.211, 2023, version 17.4.0.
- [18] K. M. Braun, “OFDM radar algorithms in mobile communication networks,” Ph.D. dissertation, Karlsruhe Institut für Technologie (KIT), 2014.
- [19] “IEEE Standard for a Precision Clock Synchronization Protocol for Networked Measurement and Control Systems,” *IEEE Std. 1588-2008*.
- [20] “Timing characteristics of synchronous equipment slave clock,” *ITU-T Rec. G.8262/Y.1362 (11/18)*.
- [21] R. E. Kalman, “A new approach to linear filtering and prediction problems,” 1960.